Ultrafast rechargeable room-temperature solid-state sodium ion battery based on graphene-based liquid alloy

QianQian Zhao
North China University of Science and Technology
Haoqing Tian
North China University of Science and Technology
Shan Liu (sliu@ncst.edu.cn)
North China University of Science and Technology https://orcid.org/0000-0002-8554-6306
Ling Wang
North China University of Science and Technology
Lei Dai
North China University of Science and Technology

Article

Keywords: batteries, solid state sodium ion batteries, energy chemistry

Posted Date: February 23rd, 2021

DOI: https://doi.org/10.21203/rs.3.rs-223685/v1

Version of Record: A version of this preprint was published at ACS Nano on May 19th, 2023. See the published version at https://doi.org/10.1021/acsnano.3c00397.

Abstract

Solid state sodium ion batteries have attracted great attentions due to its high safety and high energy density. However, the poor wettability between sodium and solid electrolytes (point-contact) seriously limits its application at room temperature. Here, we use a graphene-based Na-K alloy instead of pure sodium as anode to improve the wettability, which allows the batteries to be operated with ultrahigh rate capability at room temperature. The reduced interfacial resistance and accelerated charge transfer kinetics between alloy anode and NASICON electrolyte (face-contact) made the batteries stable cycle more than 220 hours with a small voltage hysteresis at a high current density of 25 mA cm^{-2} at room temperature, even increased the current density to 65 mA cm^{-2}, the batteries can still operate well. These results proved that the feasibility of using liquid alloy in room-temperature solid-state sodium ion batteries. This work will pave the way for the development of high-rate, dendrite-free and long-life solid-state sodium ion batteries.

Introduction

All solid-state sodium ion batteries have been widely concerned due to its high safety and high energy density in recent years[1-4]. It is fortunate that the conductivity of sodium ion conductors (NASICON[5-7], b”-alumina[8-10] and sulphide[11]) have been raised to a high enough level, about 10^{-4}~10^{-2} S cm^{-2}, at room temperature, which is approached to that of liquid electrolyte[12]. However, there are still a lot of challenges for solid-state sodium ion batteries, especially the poor wettability between sodium and electrolyte, which will increase the interfacial resistance, promote the side reaction owing to enhanced local polarization, and accelerate dendrite growth[13-15]. Thus, how to improve the wettability (or contact) between sodium and electrolyte and ensure a fast charge transport at interface is the key to the development of solid-state sodium ion batteries.

Surface coatings and introducing interlayers are common strategies to ameliorate the contact issues for solid-state sodium ion batteries at present[16-20]. These methods can effectively improve the wettability between sodium and electrolyte by ion exchange reaction or the excellent intrinsic properties (such as flexibility and extensibility of polymer[21]). But the poor physical contact (point-contact) at interface has not been fundamentally changed by above methods. In addition, the fragile interface always suffers continuous destruction and reconstruction during cycling since the sodium has a huge volume fluctuation. In this situation, the point-contact as mentioned above is bound to face many challenges, such as cracks for oxides (or alloys) layer due to mechanical stress and the growth of dendrite may pierce polymer because its lower Young's modulus, etc.

Using liquid or molten metal anode to improve wettability has already achieved commercial success in the 1970s, such as commercial high-temperature Na-S or Na-metal halide batteries[22, 23]. But the high working temperature (300~350 ^{o}C) and high reactive activity of molten alkali metal make these batteries

very inconvenient to package, and restrict its usage range greatly. How to reduce the operating temperature of these batteries has been the focus of current research.

Alkali metal alloys (Na-K, Na-Cs, Na-Rb) have low melting point and can exist in liquid form at room temperature[24]. Recently Liu et al[25] found that Na-Cs alloy anode exhibits great improvement in cycling life over those with pure sodium anode at 175 and 150 ^{o}C. Rugolo et al[26] found that it can use liquid Na-K alloy and K-b”-alumina to yield high-voltage flow batteries. However, due to the fluidity and high surface tension of liquid alloy, it always requires a relatively high temperature and additional containers, which not only affects the energy density of the batteries, but also increases the manufacturing cost of the batteries. Recently, Goodenough et al[27] found that liquid Na-K alloy can be successfully applied to room-temperature K-ion batteries with conventional liquid electrolyte, and can effectively inhibit the dendrite growth and achieve stable long cycle.

Herein, we prepared a processable graphene-based Na-K alloy anode (rGO@Na-K) which can intimate contact with NASICON-type electrolyte ($Na_3Hf_2Si_2PO_{12}$) without surface modification at room temperature. The processable Na-K alloy anode, thanks to their specific excellent adhesion, could intrinsically avoid the dendrite growth while keeping close contact with the electrolyte (Fig 1a), compared with pure sodium anode which have a point-contact with electrolyte (Fig 1b). Moreover, the faster mass transport of liquid alloy makes the batteries have an excellent rate capability. For this reason, the symmetric cells with the graphene-based Na-K alloy anode can cycle steady more than 220 hours with a small voltage hysteresis under the high current density of 25 mA cm^{-2}. Even the current density increases to 65 mA cm^{-2}, the batteries can still operate well. The full cells with alloy anode also show better performance than that with pure sodium anode. The batteries can achieve stable cycling at high rate of 10 C more than 100 cycles, even facing the higher current density of 20 C, the batteries can still cycle normally.

Results

Fabrication of processable Na-K alloy anode.

The Na-K alloy has a lower eutectic temperature about -11 ^{o}C (Supplementary Fig 1), therefore, it can exist in liquid form at room temperature. In this work, the Na-K alloy is obtained by directly stacking sodium and potassium foil according to a certain proportion (Na:K = 44:56 wt%). Due to the high surface tension of the liquid Na-K alloy, it is always a knotty problem to realize good wetting with matrix materials. This may be the reason for that liquid metal is often used in flow batteries system. To obtain a processable and packageable Na-K alloy anode, a suitable porous substrate is usually needed. Graphene materials, with light weight, excellent chemical and mechanical stability, suitable pore structure and abundant surface functional groups, are regarded as an ideal energy storage material in past years[28-30]. Beyond that, recent studies have also found that the layered graphene can effectively alleviate the volume effect of the electrode while realizing the rapid charge transfer during cycling[29, 31].

Therefore, we chose the layered graphene as the storage matrix for liquid Na-K alloy in this work (Fig 2a). The result proved that the liquid Na-K alloy can spread fast across the graphene matrix when dropped alloy droplets to the graphene matrix (Fig 2b-e, Supplementary Movie 1). The good wettability of layered graphene should be attributed to the abundant functional groups and capillary adsorption effect on graphene surface according to the literatures[32-34]. Additionally, it is worth emphasizing that the liquid alloy could quickly detached from the graphene film (Fig 2f-g) as previous studies when we immersed the prepared alloy anode into the DME (1, 2-dimethoxyethane) solvent[35, 36]. The scanning electron microscope (SEM) image and EDS mappings showed that liquid alloy was uniformly distributed in the layered graphene film (Fig 2h-k). These results proved that there is mainly based on physical adsorption between alloy and graphene matrix, which could maintain an intimate liquid-solid contact between alloy anode and solid electrolyte.

It should be noted that the rapid diffusion of the metal-ion in matrix for solid-state batteries is much more important than the batteries with liquid electrolyte, because the latter have a good fluidity and wettability. So, here we also compared the diffusion speed of the liquid alloy in different matrix materials (such as, carbon paper, carbon felt, nickel foam and copper foil, etc.). It was observed that carbon felt, nickel foam and copper foil don't show any wetting behavior with Na-K alloy at room temperature even after more than two hours (Supplementary Fig 2). Although carbon paper can be wetted, it takes more than ten minutes for alloy to spread across (Supplementary Fig 3). In addition, it should also note that the fabrication process of graphene-based Na-K alloy developed in this work has a great advantage with previous studies (Supplementary Table 1), for instance, the easy processability of Na-K alloy can be obtained quickly without high-temperature or negative-pressure[27, 37, 38].

Wetting behaviour of Na-K alloy and sodium on NASICON electrolyte.

In this work, we chose a novel NASICON-Type $Na_3Hf_2Si_2PO_{12}$ as the electrolyte, which has monoclinic structure and its conductivity can reach 1.4×10^{-3} S cm^{-2} at room temperature (Supplementary Fig 4-6). Figure 3 shows images of Na-K alloy and pure sodium on $Na_3Hf_2Si_2PO_{12}$ surface at different temperatures. Obviously, the Na-K alloy has a better wettability with $Na_3Hf_2Si_2PO_{12}$ than pure sodium whether it's at room temperature or high temperature (Fig 3a-c). Especially, graphene-based Na-K alloy can closely adhere to the $Na_3Hf_2Si_2PO_{12}$ surface at room temperature (Fig 3d). The reason for the superior wettability of alloy can be summarized as follows. Firstly, the internal bonding force of Na-K alloy is less than that of pure sodium, as the internal bonding force decreases the surface tension will decrease[39]. This is also the reason why Na-K alloy has a lower melting point (Supplementary Fig 7). Secondly, the graphene-based Na-K alloy with property of non-newtonian fluid state could realize an intimate liquid-solid contact with $Na_3Hf_2Si_2PO_{12}$ at room temperature[40]. In comparison, there must have a large interfacial resistance between pure sodium and $Na_3Hf_2Si_2PO_{12}$ electrolyte because it is a point-contact at room temperature (Fig. 3e, h). Although the contact between pure sodium and $Na_3Hf_2Si_2PO_{12}$ can change from solid-solid to liquid-solid with the temperature increased, there still have a poor wettability due to the large surface tension of molten sodium (Fig 3f-g).

To clarify the foundational wetting mechanism of Na-K alloy and pure sodium on $Na_3Hf_2Si_2PO_{12}$ electrolyte, the wetting process of two electrodes were simulated by DFT (Fig 3i-j). The classic wetting theory defined the main thermodynamic relationship among surface tension, wetting angle and adhesion work (ω_a) as follow equation[41]:

$$\cos\theta = \frac{\gamma_S - \gamma_M}{\gamma_I}$$

$$\omega_a = \gamma_I \times (1 + \cos\theta)$$

where γ_S and γ_M respectively represent the surface energy of solid electrolyte (S) and liquid metal (M), γ_I represents the interfacial energy of the interface (I) between liquid metal and solid electrolyte surface. The contact angle, q, for these interfaces were calculated by combining the above equation, with DFT calculations of the interfacial work of adhesion, ω_a, and the surface energy of NaK_3 alloy and Na. The better wettability should be directly related to a larger ratio of ω_a/s_M. Compared with pure sodium (s_{Na} = ~150 dyn cm^{-1}), the surface of potassium (s_K = ~68 dyn cm^{-1}) is much lower in the studied temperature range[21]. But the calculated ω_a for NaK_3-$Na_3Hf_2Si_2PO_{12}$ (0.185 j m^{-2}), which is larger than that for Na-$Na_3Hf_2Si_2PO_{12}$ system (0.166 j m^{-2}), based on the stronger interaction between NaK_3 alloy and $Na_3Hf_2Si_2PO_{12}$ atoms. The larger ω_a and smaller s_K for Na-K alloy mean a smaller wetting angle, therefore, the surface wettability on $Na_3Hf_2Si_2PO_{12}$ is better than that on pure sodium, as observed in the current study. However, we found that the surface tension of the alloy is still high at room temperature. Therefore, the graphene matrix plays an important role in improving the adhesion between the alloy and $Na_3Hf_2Si_2PO_{12}$.

Stability analysis of the interface between Na-K alloy and $Na_3Hf_2Si_2PO_{12}$ electrolyte.

We know that for solid-state batteries, the interface contact always faces significant challenges during cycling due to the side-reaction and volume effect of electrode. To clear whether graphene-based Na-K alloy can keep intimate contact with $Na_3Hf_2Si_2PO_{12}$ electrolyte during cycling, the batteries were disassemble and the morphologies of the interface were observed after cycling. For Na-K alloy, the graphene-based Na-K alloy still tightly adheres to the surface of $Na_3Hf_2Si_2PO_{12}$ electrolyte even after 100 cycles (Fig 4a-b). Conversely, even the surface of $Na_3Hf_2Si_2PO_{12}$ electrolyte was modifidied by tin oxide, there still has a obvious gap between sodium and the $Na_3Hf_2Si_2PO_{12}$ electrolyte after cycling (Fig. 4d-e). In addition, we also observed the existence of dendrites for pure sodium anode (Supplementary Fig 8). This should be attributed to the poor physical contact between pure sodium and solid electrolyte, huge volume fluctuations of sodium and stress generated during cycling. The result also be testified by the electrochemical impedance spectroscopy (EIS) and X-ray photoelectron spectroscopy (XPS) test. When pure sodium anode was substituted with graphene-based Na-K alloy, the interface resistance between

anode and $Na_3Hf_2Si_2PO_{12}$ decreased significantly from 105 Ω cm^2 to 15 Ω cm^2. (Supplementary Fig 9). Additionally, for Na-K alloy anode, no peak shift can be observed (Fig 4c), indicating that there has a more stable interface between Na-K alloy and $Na_3Zr_2Si_2PO_{12}$. But for sodium anode, there has a obvious peak of Hf 4f shift appears after the cycling (Fig 4f), indicating that there have a unstable interface between sodium and $Na_3Hf_2Si_2PO_{12}$. This is because the liquid alloy can keep a good adhesion with the solid electrolyte, the influence of local polarization on the electrolyte interface is avoided, so the long-term stability of the interface can be realized.

Electrochemistry performance of graphene-based Na-K alloy anode.

The electrochemistry performance of graphene-based Na-K alloy anode and pure sodium anode were evaluated with symmetric cells and full cells. The symmetric cells with alloy anode could cycle stably more than 220 hours with a small voltage hysteresis about 8 mV at current density of 25 mA cm^{-2} (Fig 5a). When the current density is increased to 40 mA cm^{-2}, the symmetric cells still exhibit very stable cycling with a small overpotential (Fig 5b). This is the best value for solid state sodium batteries at room temperature so far (Fig 5c, Supplementary table 2). As discussed above, the reason for this excellent performance should attribute to the intimate contact between graphene-based Na-K alloy and $Na_3Hf_2Si_2PO_{12}$ electrolyte, which could effectively reduce the interface resistance and accelerated mass/charge transfer dynamics. In sharp contrast, the batteries with pure sodium anode can't work normally even at a low current density of 0.1 mA cm^{-2} (Supplementary Fig 10).

Additionally, the rate performance of Na-K alloy and pure sodium were also compared. For Na-K alloy anode, the current density of the symmetric cells can up to 65 mA cm^{-2} (Fig 5d), this value have equally matched to the high-temperature Na-S batteries or flow batteries. On the contrary, for pure sodium anode, even the surface of $Na_3Hf_2Si_2PO_{12}$ has been modified with tin oxide by ion plating, the limiting current is only 1.0 mA cm^{-2} (Supplementary Fig 11). The full cells of Na-K/$Na_3Hf_2Si_2PO_{12}$/$Na_3V_2(PO_4)_3$ were also tested, and compared with pure sodium anode. The batteries of Na-K/$Na_3Hf_2Si_2PO_{12}$/$Na_3V_2(PO_4)_3$ could steady cycle more than 100 cycles without capacity fading at 5 C and 10 C (Supplementary Fig 12 and Fig 5e). Even the current density increase to 20 C, the batteries can still cycle normally (Fig 5f). But for pure sodium anode, when increase the current rate to 10 C, there have a smaller discharge capacity than the alloy full cell and the polarization increased significantly, which can be attributed to the point contact between pure sodium and $Na_3Hf_2Si_2PO_{12}$ (Supplementary Fig 13).

Discussion

In summary, we prepared an ultrafast rechargeable room-temperature solid state sodium ion battteries based on liquid Na-K alloy and NASICON electrolyte $Na_3Hf_2Si_2PO_{12}$. The flowability of Na-K alloy anode could achieve an intimate contact with $Na_3Hf_2Si_2PO_{12}$ electrolyte, which could guarantee uniform charge distribution, rapid mass/charge transfer kinetics and efficiently inhibit side reactions at the interface. Based on above reasons, the symmetrical cells with Na-K alloy anode exhibit an excellent rate

performance, which could cycle stability more than 220 hours at current density of 25 mA cm^{-2}. Even the current density increases to an ultra-high value about 65 mA cm^{-2}, there are still no obvious short circuit. The full cell of Na-K/$Na_3Hf_2Si_2PO_{12}$/$Na_3V_2(PO_4)_3$ can provide a specific capacity of 106 mAh g^{-1} at a high rate of 10 C. Moreover, it maintained a high-capacity retention of 99% after 100 cycles. This work gives a robust method to construct stable interface between anode and solid electrolyte and suggests a straightforward pathway to achieve high energy and power density solid-state batteries.

Methods

NASICON-type electrolyte fabrication. The pristine $Na_3Hf_2Si_2PO_{12}$ powder with small particles was prepared by high temperature solid phase reaction method. Na_2CO_3 (99.8%), HfO_2 (99.8%), SiO_2 (99.9%), and $NH_4H_2PO_4$ (99.9%) with the stoichiometric ratio were used as the reagent materials and dissolved into the absolute ethanol. The mixture was ball-milled for 48 hours and then fired at 900 ^oC. The resulting powder was further put into a mold to get the pellets under 10 MPa pressure, then formed by cold isostatic pressing. The dense $Na_3Hf_2Si_2PO_{12}$ pellets were finally formed by sintering at the temperature of 1250 °C for 24 h. The diameter of the obtained $Na_3Hf_2Si_2PO_{12}$ pellet is 11 mm and the thickness is at the range of 1-1.2 mm. The prepared pellets were polished for use. The surface of $Na_3Hf_2Si_2PO_{12}$ was coated with tin layer by ion sputtering in vacuum. The thickness of the obtained tin layer was ≈ 20 nm, the chamber vacuum is below 10^{-4} Pa and the current is 20 mA. Then the tin coated electrolyte pellets were sintered at 900 °C for 3 hours to oxidize tin to tin oxide.

Fabrication of processable Na-K alloy electrode. The Na-K liquid alloy was fabricated by a facile room temperature alloying process. In a typical synthesis, 44 wt% sodium and 56 wt% potassium were physically stacked together to form liquid Na-K alloy. To prepare graphene-based Na-K alloy electrode (rGO@Na-K), the graphene oxide (GO) film is obtained by suction filtration. At first, take 5 mL of graphene aqueous dispersion for suction filtration and dry overnight at 60 °C. Secondly, peel off from the filter membrane and reduce graphene oxide at 350 °C under argon protection to remove excess functional groups. At last, drop the liquid Na-K alloy on the reduced graphene oxide (rGO) film to form graphene-based Na-K alloy electrode at room temperature.

Computational modelling. Calculations were performed using the Materials Studios based on the DFT, employing the projector augmented wave (PAW) method as the potentials, and the Perdew-Burke-Ernzerhof (PBE) generalized-gradient approximation (GGA). For structural relaxation and energy/density of states calculations, the energy cutoff of 520 eV and 4×4×1 K-point Monkhorst-Pack grid were used. The convergence criterion of energy and force for structural relaxation were set as 1.0×10^{-5} eV and 0.01 eV/Å, respectively. All stoichiometric structures were taken from the Materials Project (https://www.materialsproject.org/). For $Na_3Hf_2Si_2PO_{12}$, eight times supercells were used for non-stoichiometric ratio. In order to investigate the interphase of Na-K alloy or pure sodium anode with electrolyte, NaK_3 (110)/NASICON (110) and Na (110)/NASICON (110) interphases were built.

Cells construction and testing. The $Na_3V_2(PO_4)_3$ cathode included 30 wt% $Na_3V_2(PO_4)_3$ sample, 65 wt% Super P, and 5 wt% PVDF on an Al foil, and its mass loading was around 1.3 mg cm^{-2}. The electrolyte of 1 M $NaClO_4$ in EC: DMC: EMC = 1:1:1 (5% FEC) about 10 μL was added at the interface between the $Na_3V_2(PO_4)_3$ cathode and the $Na_3Hf_2Si_2PO_{12}$ pellet to assemble the full cells. The $Na_3V_2(PO_4)_3$ powder was prepared by the solvent evaporation method. V_2O_5 (99.8%), Na_2CO_3 (99.8%), $NH_4H_2PO_4$ (99.9%) and citric acid (99.9%) with the stoichiometric ratio of 2:3:6:3 were dissolved into the deionized water, then steamed it to dry at 80 °C. Before sintering, firstly heated at 350 °C for 4 h, then reacted at 800 °C for 12 h under an argon atmosphere.

Material characterization. Morphologies of samples were characterized by scanning electron microscope (SEM, Hitachi S4800) coupled with EDS. The XRD patterns were texted by Riguka D/max 2500/PC diffract meter using Cu Kα radiation (λ = 1.5418 Å), the angle range is 10-90° (2θ). The XPS spectras ware examined by PHI5802 to analyze the different valence states of Hf element, and the binding energies were referenced to the C 1s energy of 284.6 eV. All samples were prepared in a glove box. The impedance of batteries was obtained by EIS in the frequency range of 100 kHz to 0.01 Hz with a voltage amplitude of 10 mV. The charge-discharge datas were obtained on a Land 2001A battery testing system.

Declarations

Acknowledgements

The authors appreciate support from Basic Scientific Research Natural Science Foundation of China (No.52004092, 51872090).

Author contributions

S. L and L. W. conceived and designed the experiments. Q.Q.Z synthesized and characterized the materials, and performed the experiments. S. L conceived the simulation protocol, and carried out the simulations. S. L. and L. W. analysed the date, and S. L. wrote the manuscript. L. D. and H.Q. T. discussed the results and commented on the manuscript.

Additional information

Supplementary Information accompanies this paper at http://www.nature.com/ nature communications.

References

1. Fu, H. *et al.* Reducing interfacial resistance by Na-SiO_2 composite anode for NASICON-based solid-state sodium battery. *ACS Mater. Lett.* **2**, 127-132 (2019).

2. Lu, Y. *et al.* A high-performance monolithic solid-state sodium battery with Ca^{2+} doped $Na_3Zr_2Si_2PO_{12}$ electrolyte. *Adv. Energy Mater.* **9**, 1901205 (2019).

3. Gao, H., Xue, L., Xin, S., Park, K. & Goodenough, J. B. A plastic-crystal electrolyte interphase for all-solid-state sodium batteries. *Angew. Chem. Int. Ed. Engl.* **129**, 5541-5545 (2017).

4. Liu, L. *et al.* In situ formation of a stable interface in solid-state batteries. *ACS Energy Lett.* **4**, 1650-1657 (2019).

5. Gao, Z., Yang, J., Yuan, H., Fu, H. & Huang, Y. Stabilizing $Na_3Zr_2Si_2PO_{12}$/Na interfacial performance by introducing a clean and Na-deficient s *Chem. Mater.* **32**, 3970-3979 (2020).

6. Ling, W. *et al.* A flexible solid electrolyte with multilayer structure for sodium metal batteries. *Adv. Energy Mater.* **10**, 1903966 (2020).

7. Zang, Z. *et al.* A self-forming composite electrolyte for solid-state sodium battery with ultralong cycle life. *Adv. Energy Mater.* **7**, 1601196 (2016).

8. Lu, X. *et al.* Liquid-metal electrode to enable ultra-low temperature sodium-beta alumina batteries for renewable energy storage. *Nat. Com* **5**, 4578 (2014).

9. Hee-Jung, C. *et al.* Decorating β"-alumina solid-state electrolyte with submicron Pb spherical particles for improving Na wettability at lower temperatues. *J. Mater. Chem. A.* **6**, 19703-19711 (2018).

10. Xiao, C. *et al.* A high-energy quinone-based all-solid-state sodium metal battery. *Nano Energy* **62**, 718-724 (2019).

11. Hayashi, A., Noi, K., Sakuda, A. & Tatsumisago, M. Superionic glass-ceramic electrolytes for room-temperature rechargeable sodium batteries. *Nat. Commun.* **3**, 856 (2011).

12. Ling, W. *et al.* A flexible solid electrolyte with multilayer structure for sodium metal b *Adv. Energy Mater.* **10**, 1903966 (2020).

13. Zhou, W., Li, Y., Xin, S. & Goodenough, J. Rechargeable sodium all-solid-state battery. *ACS Cen. Sci.* **3**, 52-57 (2017).

14. Uchida, Y. *et al.* Insights into sodium-ion transfer at Na/NASICON interface improved by uniaxial c *ACS Appl. Energy Mater.* **2**, 2913-2920(2019).

15. Tian, Y. *et al.* Reactivity-guided interface design in Na metal solid-state b *Joule* **3**, 1037-1050 (2019).

16. Yang, J. *et al.* Guided-formation of a favorable interface for stabilizing Na metal solid-state batteries. *J. Mate Chem. A.* **8**, 7828-7835 (2020).

17. Matios, E. *et al.* Graphene regulated ceramic electrolyte for solid-state sodium metal battery with superior electrochemical s *ACS Appl. Mater. Interfaces.* **11**, 5064-5072 (2019).

18. Miao, X. *et al.* AlF_3-modified anode-electrolyte interface for effective Na dendrites restriction in NASICON-based solid-state electrolyte. *Energy Storage Mater.* **30**, 170-178 (2020).

19. Gross, M. *et al.* Tin-based ionic chaperone phases to improve low temperature molten sodium-NaSICON interfaces. *J. Mater. Chem. A.* **8**, 17012-17018 (2020).

20. Zhang, S., Zhao, Y., Zhao, F., Zhang, L. & Sun, X. Gradiently sodiated alucone as an interfacial stabilizing strategy for solid-state Na metal b *Adv. Funct. Mater.* **30**, 2001118 (2020).

21. Yu, X. & Manthiram, A. Sodium-sulfur batteries with a polymer-coated NASICON-type sodium-ion solid e *Matter* **1**, 439-451 (2019).

22. Hueso, K. , Armand, M. & Rojo, T. High temperature sodium batteries: status, challenges and future trends. *Energy Environ. Sci.* **6**, 734-749 (2013).

23. Small, L. *et al.* Next generation molten NaI batteries for grid scale energy storage. *J. Power Sources.* **360**, 569-574 (2017).

24. Liu, H., Cheng, X., Huang, J., Kaskel, S. & Zhang, Q. Alloy anodes for rechargeable alkali-metal batteries: progress and c *ACS Materials Lett.* **1**, 217-229 (2019).

25. Lu, X. *et al.* Liquid-metal electrode to enable ultra-low temperature sodium-beta alumina batteries for renewable energy storage. *Nat. Commun.* **5**, 4578 (2014).

26. Baclig, A. *et al.* High-voltage, room-temperature liquid metal flow battery enabled by Na-K|K-β"-alumina stability. *Joule* **2**, 1287-1296 (2018).

27. Xue, L. *et al.* Liquid K-Na alloy anode enables dendrite-free potassium b *Adv. Mater.* **28**, 9608-9612 (2016).

28. Liu, L. *et al.* 3D rGO aerogel with superior electrochemical performance for K-ion battery. *Energy Storage Mater.* **19**, 306-313 (2019).

29. Lin, D. *et al.* Layered reduced graphene oxide with nanoscale interlayer gaps as a stable host for lithium metal anodes. *Nat. Nano.* **11**, 626-632 (2016).

30. Yi, Z., Qian, Y., Jiang, S., Li, Y. & Qian, Y. Self-wrinkled graphene as a mechanical buffer: A rational design to boost the K-ion storage performance of Sb_2Se_3 *Chem Eng J.* **379**, 122352 (2019).

31. Wang, A., Hu, X., Tang, H., Zhang, C. & Luo, J. Processable and moldable sodium-metal anodes. *Angew. Chem. Int. Ed.* **56**, 11921-11926 (2017).

32. Zhang, L. *et al.* Graphite intercalation compound associated with liquid Na-K towards ultra-stable and high-capacity alkali metal a *Energy Environ. Sci.* **12**, 1989-1998 (2019).

33. Qin, L. *et al.* Graphene-directed formation of a nitrogen-doped porous carbon sheet with high catalytic performance for the oxygen reduction r *J. phys. chem. C.* **122**, 13508-13514 (2018).

34. Qin, L. *et al.* Capillary encapsulation of metallic potassium in aligned carbon nanotubes for use as stable potassium metal a *Adv. Energy Mater.* **9**, 1901427 (2019).

35. Xue, L. *et al.* Room-temperature liquid Na-K anode m *Angew. Chem. Int. Ed. Engl* **57**, 14184-14187 (2018).

36. Ding, Y. *et al.* Room-temperature all-liquid-metal batteries based on fusible alloys with regulated interfacial chemistry and w *Adv. Mater.* **32**, 2002577 (2020).

37. Zhang, L. *et al.* Exploring self-healing liquid Na-K alloy for dendrite-free electrochemical energy s *Adv. Mater.* **30**, 1804011 (2018).

38. Xie, Y., Hu, J. & Zhang, Z. A stable carbon host engineering surface defects for room-temperature liquid Na-K anode. *J. Electroanalytical Chem.* **856**, 113676 (2020).

39. Zheng, Z., Ye, H. & Guo, Z. Recent progress in designing stable composite lithium anodes with improved w *Adv. Sci.***7***, 2002212* (2020).

40. Zhang, L. *et al.* Non-newtonian fluid state K-Na alloy for a stretchable energy storage d *Small Methods* **3**, 1900383. (2019).

41. Guo, X., Zhang, L., Ding, Y., Goodenough, J. & Yu, G. Room-temperature liquid metal and alloy systems for energy storage applications. *Energy Environ. Sci.* **12**, 2605-2619 (2019).

Figures

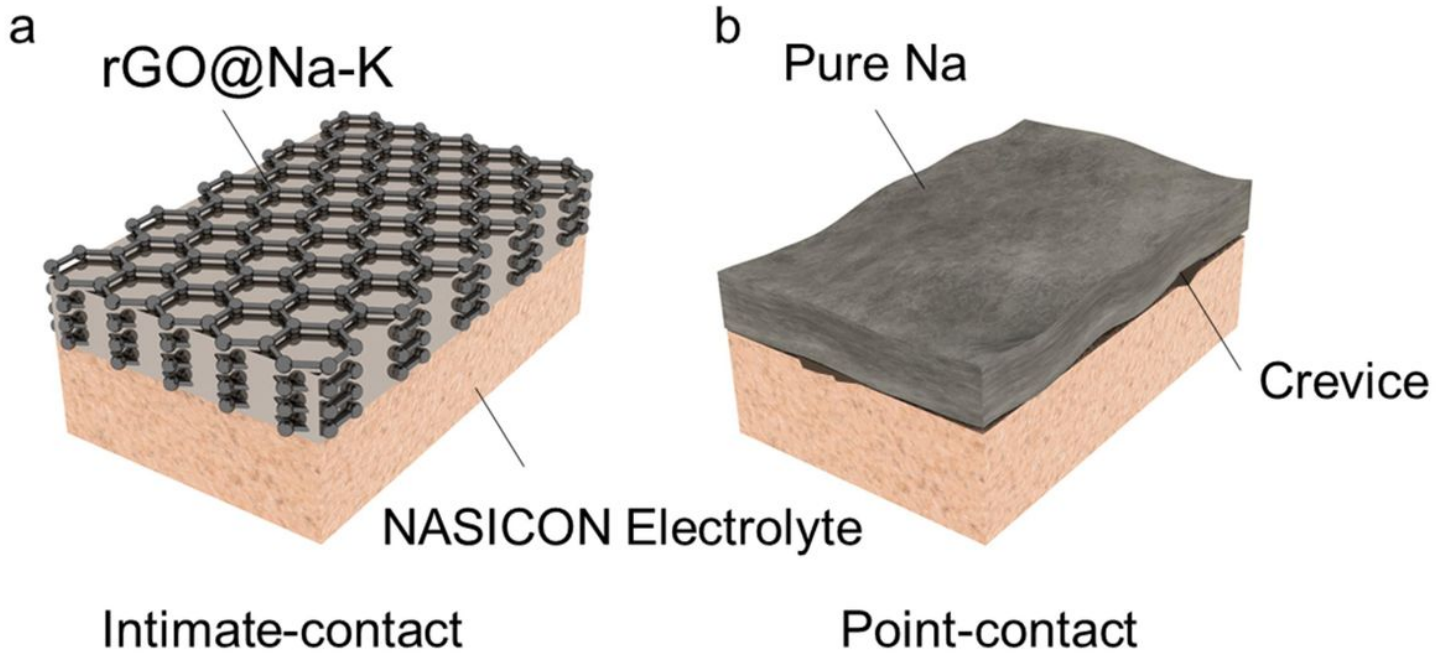

Figure 1

The schematic of the interface contact of solid electrolyte with graphene-based Na-K alloy anode and pure sodium anode. a The intimate contact between liquid Na-K alloy and solid electrolyte could reduce side effects, effectively optimize the mass transfer kinetics at interface and intrinsically avoid the dendrite growth. b In contrast, the larger interface resistance and unhomogeneous charge distribution, as a result of the poor point-contact between the pure sodium anode and solid electrolyte, which may accelerate the side reaction and dendrite penetration.

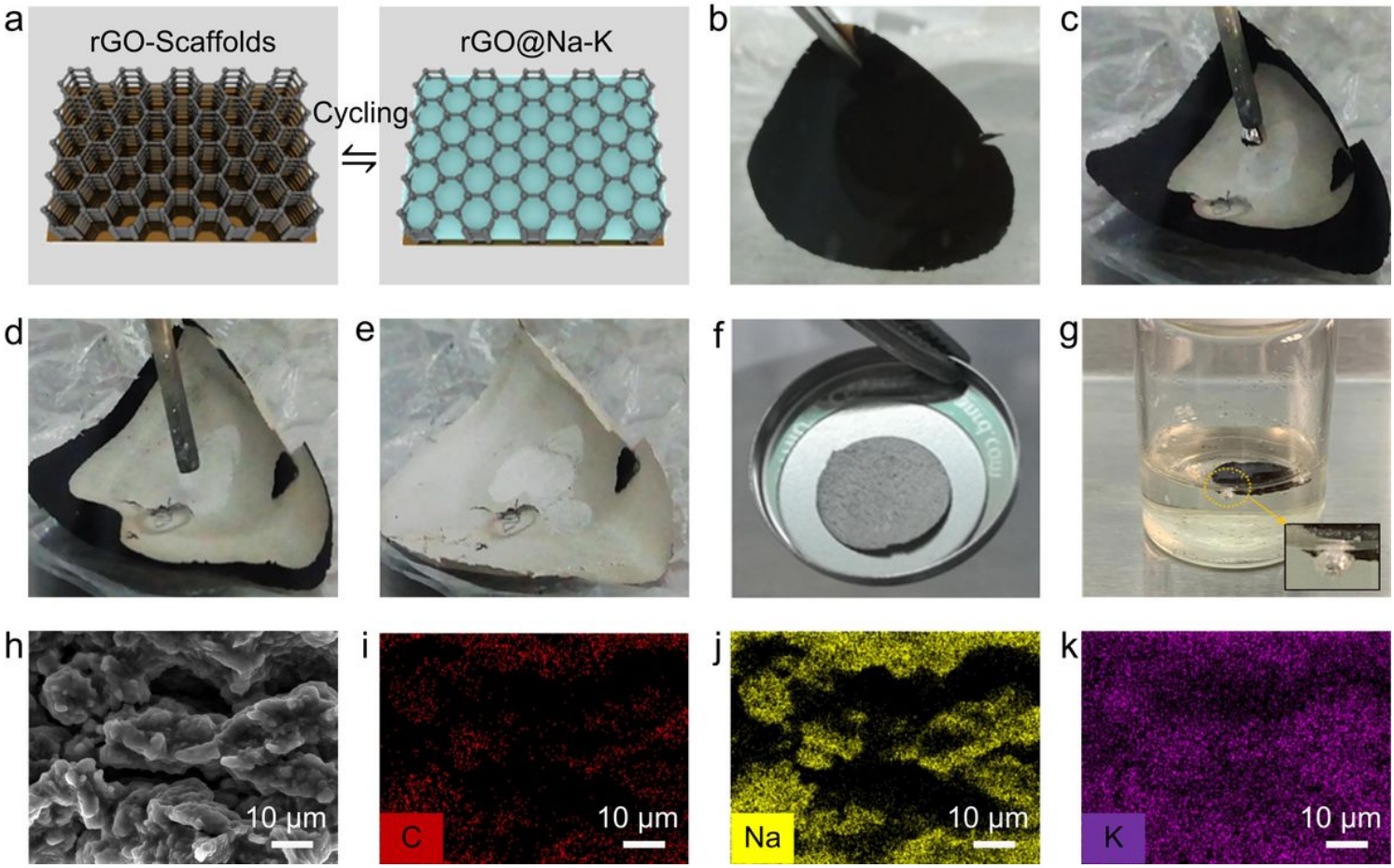

Figure 2

Fabrication of processable Na-K alloy anode. a Schematic of the layered graphene and rGO@Na-K anode. b-e Wetting process of liquid Na-K alloy on layered graphene. f, g The anode is immersed in DME, and the Na-K alloy is quickly precipitated from layered graphene the enlarged part shows the precipitated Na-K alloy. h-k Cross-section SEM image and mappings of rGO@Na-K anode. The layered structure is maintained, and the sodium and potassium elements are evenly dispersed.

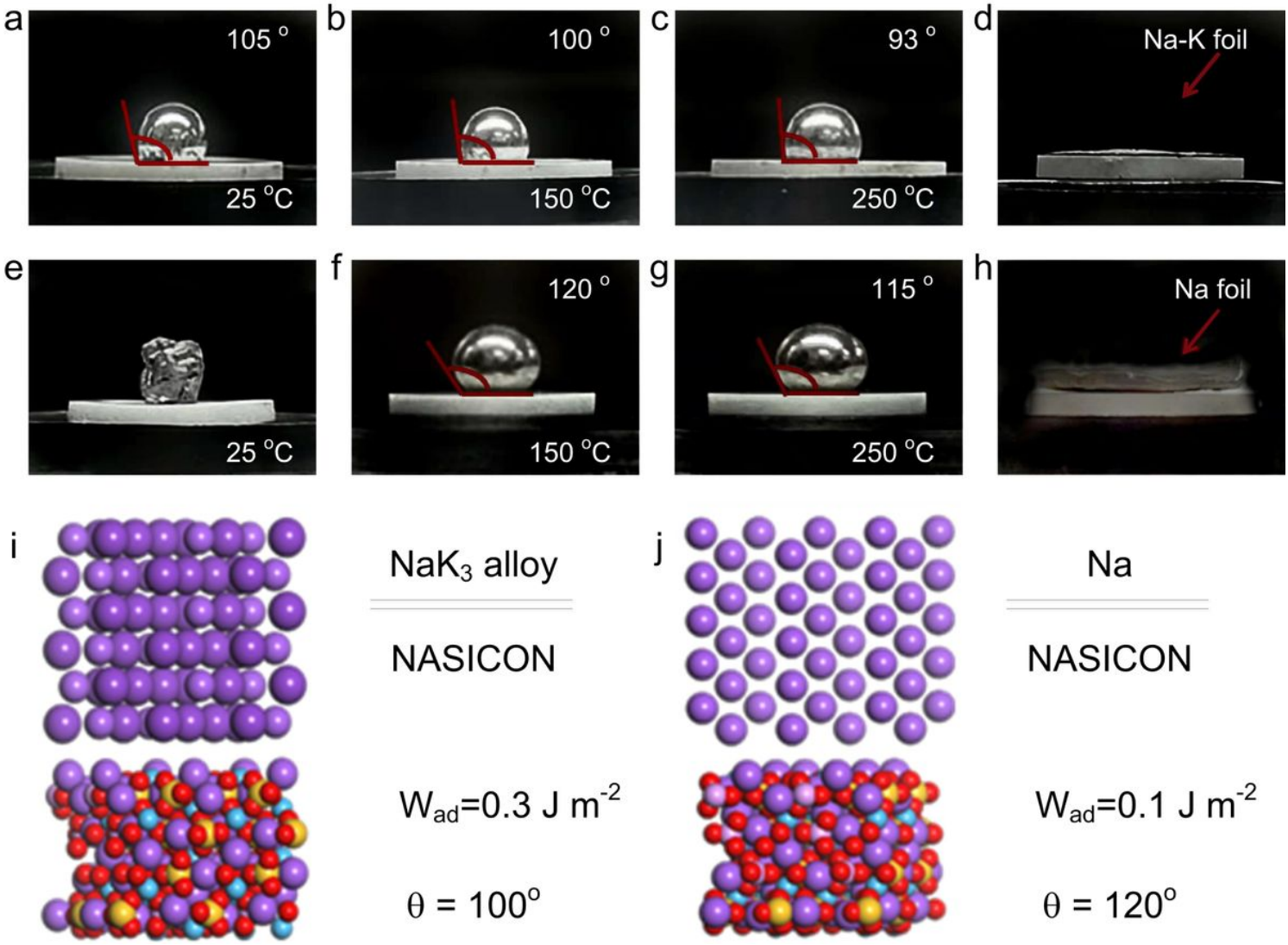

Figure 3

Wetting behaviour of Na-K alloy and sodium on Na3Hf2Si2PO12 surface and computational modelling of them. a-c Contact angle measurements of Na-K alloy on Na3Hf2Si2PO12 surface at vairous temperatures. d Image of direct contact between graphene-based Na-K alloy foil and Na3Hf2Si2PO12. e-g Contact angle measurement of pure sodium on Na3Hf2Si2PO12 surface at various temperatures. h Image of interface contact between pure sodium foil and Na3Hf2Si2PO12. i, j The atomic structure of the interface energy for NaK3-Na3Hf2Si2PO12 and Na-Na3Hf2Si2PO12.

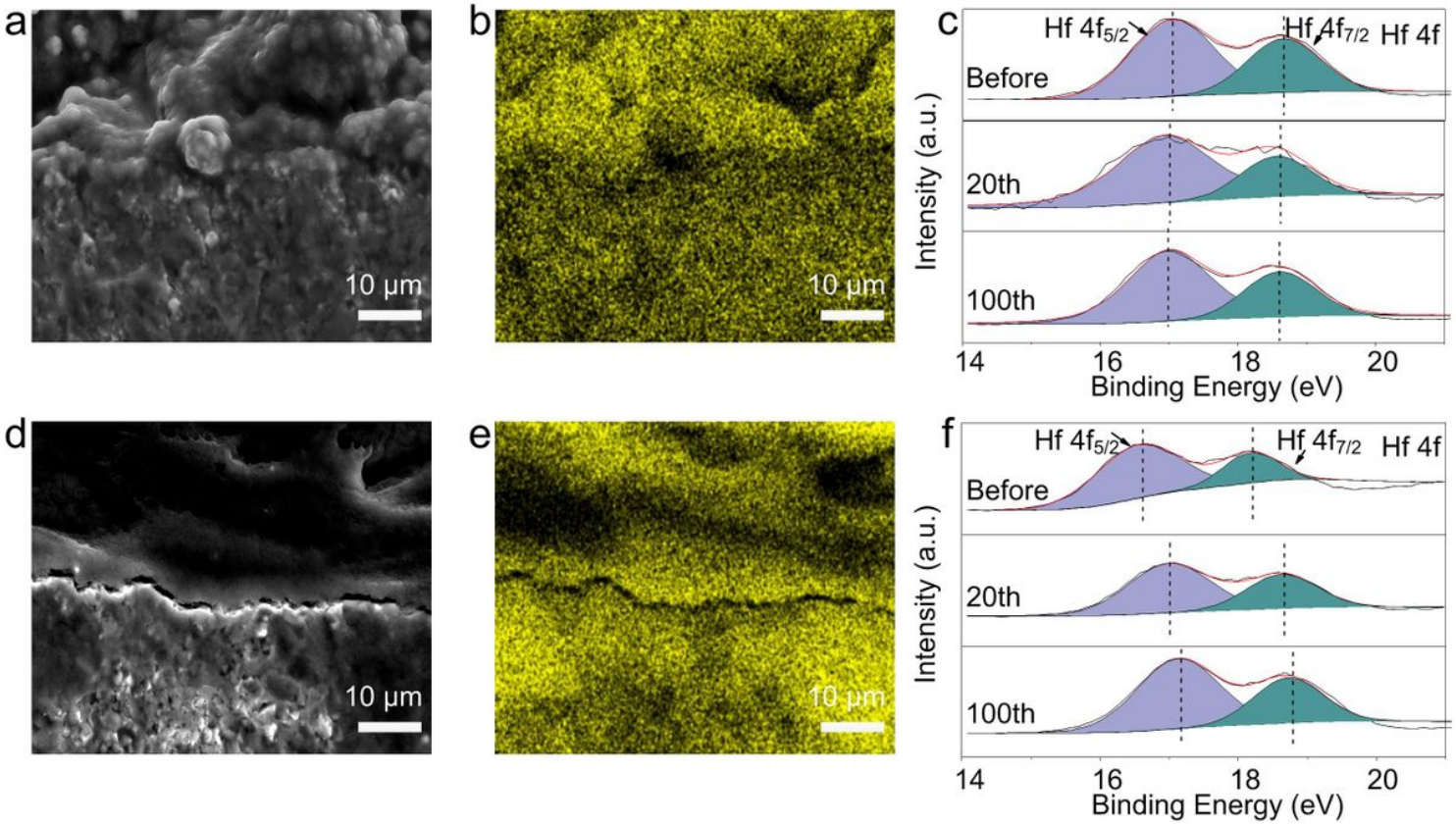

Figure 4

Stability analysis of the interface between Na-K alloy and Na3Hf2Si2PO12 electrolyte. a, b Cross-section SEM and corresponds mapping images of interface contact between Na-K alloy and Na3Hf2Si2PO12 after cycling 100 cycles. c Hf 4f XPS spectra of the Na-K/Na3Hf2Si2PO12 interface before and after cycling. d, e Cross-section SEM and corresponds mapping images of interface contact between pure sodium and Na3Hf2Si2PO12 after cycling 100 cycles. f Hf 4f XPS spectra of the Na/Na3Hf2Si2PO12 interface before and after cycling.

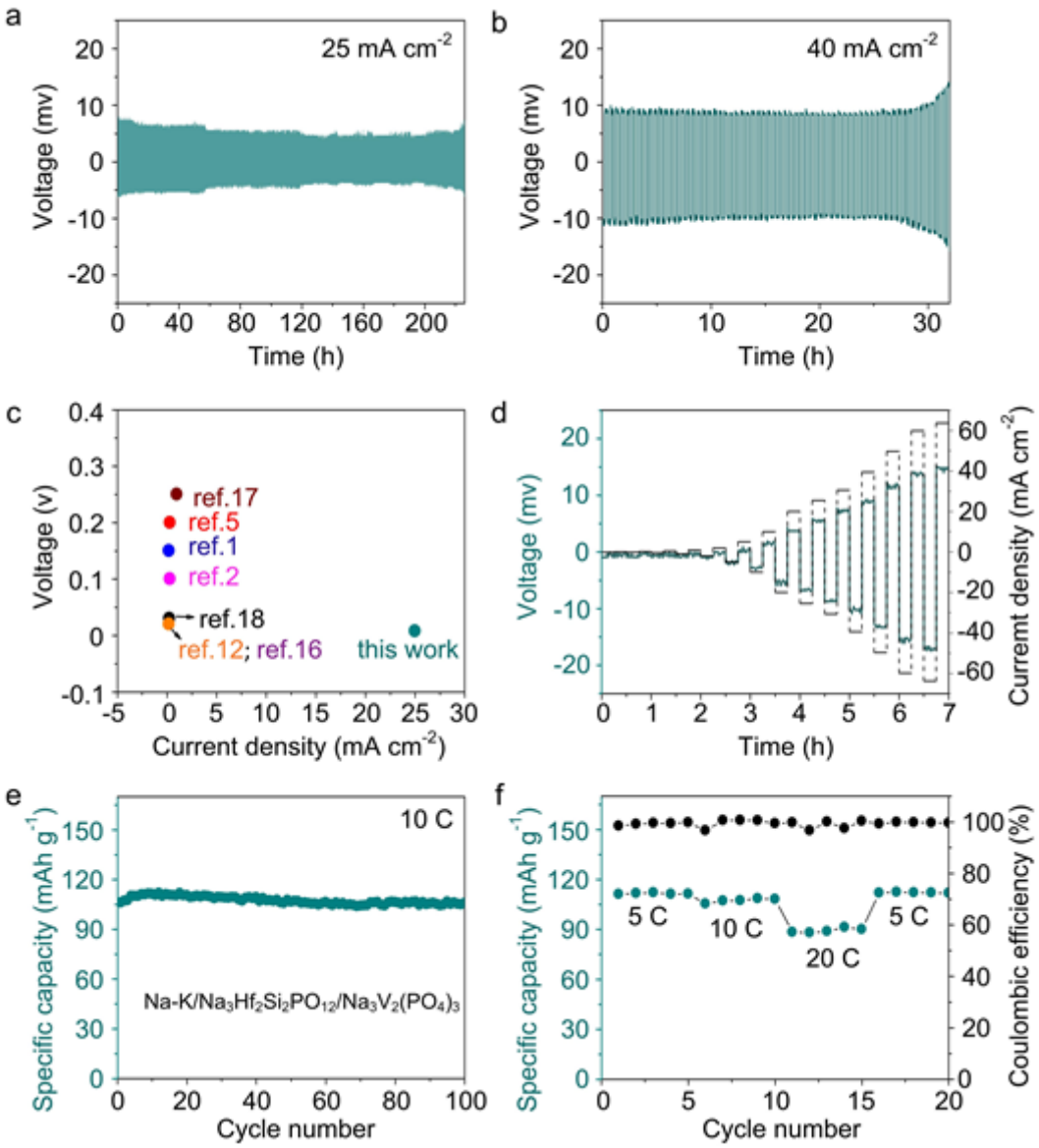

Figure 5

Electrochemical characterization of the Na-K alloy anode. Galvanostatic cycling performance of the Na-K/Na3Hf2Si2PO12/Na-K symmetric cell under a 25 mA cm-2 and b 40 mA cm-2. c Contrast the current density (x-axis), overpotential value (y-axis) of existing solid state sodium battreies based NASICON-type electrolyte with our work. d Voltage-time profile of Na-K/Na3Hf2Si2PO12/Na-K symmetric cell on galvanostatic cycling with stepped current density. e Cycling profile of the full cell of Na-K/Na3Hf2Si2PO12/Na3V2(PO4)3 at 10 C. f Rate performance of the full cell.

Supplementary Files

This is a list of supplementary files associated with this preprint. Click to download.

- SupportingInformation.doc

- Movie1.mp4